# New Generation of Tunable Bioactive Shape Memory Mats Integrated with Genetically Engineered Proteins

Xiaowen Wu, Suntharavathanan Mahalingam, Sarah Kay VanOosten,
Cate Wisdom, Candan Tamerler, Mohan Edirisinghe*

Aligned poly(ʟ-lactide)/poly(methyl methacrylate) binary blend fibers and mats loaded with a chimeric green fluorescence protein having a bioactive peptide with hydroxyapatite binding and mineralization property are prepared by pressurized gyration. The effect of processing parameters on the product morphologies, and the shape memory properties of these samples are investigated. Integration of hydroxyapatite nanoparticles into the fiber assembly is self-directed using the hydroxyapatite-binding property of the peptide genetically engineered to green fluorescence protein. Fluorescence microscopy analysis corroborated with Fourier transform infrared spectroscopy (FTIR) data confirms the integration of the chimeric protein with the fibers. An enzyme based remineralization assay is conducted to study the effects of peptide-mediated mineralization within the fiber mats. Raman and FTIR spectral changes observed following the peptide-mediated mineralization provides an initial step toward a soft-hard material transition. These results show that programmable shape memory properties can be obtained by incorporating genetically engineered bioactive peptide domains into polymer fibers.
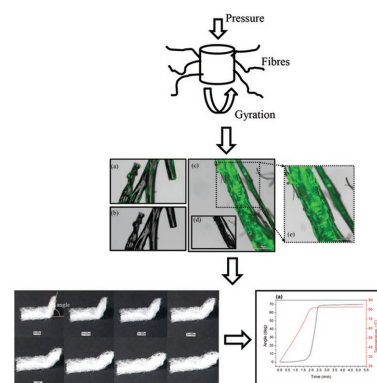
1. Introduction

Shape memory polymers (SMPs) are a class of smart materials that are able to change their shape in response to an environmental stimulus such as temperature, pH, mois-ture, or light. SMPs have been used in many fields including biomedical applications,[1] especially for minimally invasive surgery.[2] Among the numerous SMPs, poly(ʟ-lactide)/poly(methyl methacrylate) (PLLA/PMMA) are recognized as promising thermally activated SMPs with multi-shape

Dr. X. Wu
Beijing Key Laboratory of Materials Utilization of
Nonmetallic Minerals and Solid Wastes
National Laboratory of Mineral Materials
School of Materials Science and Technology
China University of Geosciences
29 Xueyuan Road, Beijing 100083, China
Dr. X. Wu, Dr. S. Mahalingam, Prof. M. Edirisinghe
Department of Mechanical Engineering
University College London
Torrington Place, London WC1E 7JE, UK
E-mail: m.edirisinghe@ucl.ac.uk

S. K. VanOosten, C. Wisdom, Prof. C. Tamerler
Bioengineering Research Center (BERC)
Department of Mechanical Engineering
University of Kansas (KU)
Lawrence, KS 66045, USA

memory properties.[3] A new stereo complex crystal was found to be formed between structurally dissimilar chiral PLLA and syndiotactic PMMA.[4] Miscible or immiscible PLLA/PMMA blends could be produced by using different processing conditions such as polymerizing the acrylic monomer in the presence of PLLA or by melt mixing the two polymers (PLLA and PMMA) in bulk.[5,6]

The solvent-casting process has been able to produce immiscible blends with matrix droplet or continuous morphologies by changing the blend composition, while extrusion melt-processing could obtain miscible PLLA/PMMA blends in a range of compositions.[7] Phase separation method with solutions of two incompatible polydisperse polymers (PLLA/PMMA) in a common solvent (e.g., chloroform) have been studied and revealed new fundamental features such as phase-in-phase or double phase morphology which are absent for solutions of just one polymer with broad molecular weight distribution in a single solvent.[8] A tri-block copolymer of PMMA/PLLA/PMMA was also synthesized and reported to have unique structure and properties.[9] Based on that, PLLA/PMMA blends were shown to be crystallized even at a low temperature of 0 °C under high pressure carbon dioxide. The effect of carbon dioxide on the crystallization behavior and the mechanical properties of PLLA/PMMA blends with various weight fraction of PMMA have been investigated.[10]

Pressurized gyration is one of the promising techniques to successfully form continuous nanofibers and functional microbubbles and capsules on a large scale.[11–13] Over the last two years, it has been a catapult to processing and forming many novel functional materials for biomedical engineering and drug delivery applications.[14–18] This technique relies on centrifugal force and dynamic fluid flow across a small orifice to create instability of a polymer or polymer/protein liquid jet at the liquid–air interface to form the desired products. In addition, by changing the physical properties of the solute–solvent mixture (e.g., surface tension, viscosity) and the processing parameters such as rotating speed and working pressure, the size, size distribution and the morphology of the products could be tailored.[11–13]

The ability to fabricate mechanically active scaffolds with additional biochemical properties presents an intriguing and innovative design opportunity. Herein, we have focused on the directed, self-assembled mineralization properties of such SMP scaffolds incorporated with a mineral-binding peptide to repair bone defects by providing local stimulation for bone tissue development. We produced these bioactive scaffolds by incorporating a genetically engineered fusion protein, which features a green fluorescence protein tag conjugated with hydroxyapatite binding and mineralization peptide (GFP-HABP). Monitoring localization of the HABP within the fiber scaffolds was performed using GFP. The presence of the bioactive HABP peptide provides control over nucleation and growth of minerals integrated into the PLLA/PMMA scaffold. An enzyme based biomineralization assay was performed to mimic the cellular environment; alkaline phosphatase (AP) was introduced to cleave phosphate groups, catalyzing mineral formation in a calcium rich buffer. In the present study, PLLA/PMMA fibers with or without the GFP-HABP fusion protein were successfully fabricated by using pressurized gyration. The morphology and the shape memory effect of the fiber mats were investigated. Following biomineralization assay, the chemical modification and microstructural changes in the fibers were investigated toward developing a tunable soft to hard matter transition in the shape memory fibers and mats.

2. Experimental Section

2.1. Materials

PLLA (amine terminated, average Mn 2500, polydispersity ≤ 1.3), PMMA (average Mn 1 20 000) were obtained from Sigma-Aldrich, UK. Chloroform with density of 1489 kg·m^{-3} at 25 °C was used as the solvent. Hydroxyapatite nanopowder (particle size ≤ 200 nm) was purchased from Sigma-Aldrich, UK and it was used as received without any modification.

2.2. Preparation of PLLA/PMMA-Based Fibers

A solution of PLLA/PMMA with composition of 50:50 weight ratio and concentration of 20 wt% in chloroform was prepared in an air tight bottle at ambient temperature (25 °C). Phosphate buffer saline solution, pH 7.4, was prepared at ambient temperature and added to the purified GFP-HABP engineered protein to achieve a working stock solution of 200×10^{-6} M. GFP-HABP was produced and purified following methods established by Yuca et al.[19] Next, a hydroxyapatite particle solution was added to the protein solution and allowed to incubate under gentle agitation to ensure peptide–particle functionalization. 15 g of PLLA/PMMA solution was taken in an air-tight bottle and 0.4 mL of the hydroxyapatite–protein mixture was added while sonicating in a water bath using an ultrasound sonifier (Branson sonifier 250) at a power output of 60% for 15 min. This prevented aggregation of the functionalized hydroxyapatite nanoparticles in the polymer solution.

2.3. Pressurized Gyration

Figure 1 shows the experimental set up of pressurized gyration and the resulting shape memory polymer fibers. The process of pressurized gyration and the theory of the fiber forming have been described in detail elsewhere.[11] A video of the forming illustrated in Figure 1 is given as Supporting Information.

2.4. Biomineralization

Mineral formation was performed using an AP enzyme-dependent mineralization assay.[20] Briefly, PLLA/PMMA fibers

ADVANCED
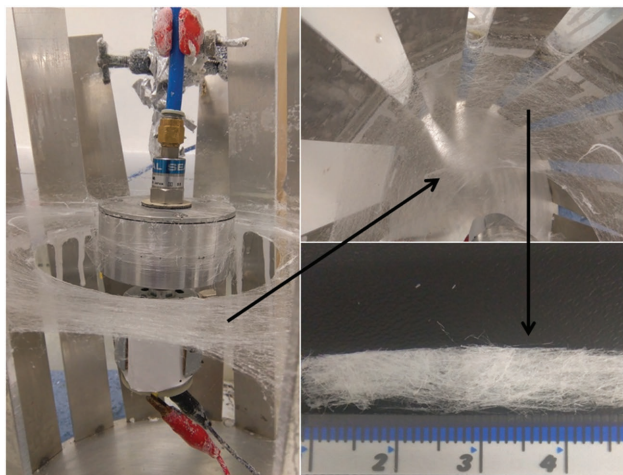SCIENCE NEWS

www.advancedsciencenews.com

Figure 1. The pressurized gyration experimental set-up and the produced shape memory polymer fibers/mats.

were incubated in a biomineralization buffer (24×10^{-3} M $CaCl_2$, 14.4×10^{-3} M b-GP, 25×10^{-3} M Tris–HCl, pH 7.4). β-GPO_4 was hydrolyzed following the addition of AP enzyme, releasing inorganic phosphate ions into the buffer rich in calcium ions which allowed for the Ca/PO_4 mineral formation. Fibers with and without GFP-HABP were incubated at 37 °C under gentle shaking in micro-centrifuge tubes containing biomineralization buffer following the addition of AP enzyme. After 24 h, the sample removed from the incubator and AP enzyme was inactivated by heating the tubes to 75 °C for 5 min.

2.5. Characterization

2.5.1. Morphology

Fibers produced were studied using field emission scanning electron microscopy with an accelerating voltage of 5 kV. Samples were coated with gold using a sputtering machine (sputter time ≈75 s) before loading to the microscope. High and low magnification images were acquired at randomly selected positions (>20) within a sample. About 150 measurements were made at random locations to plot the fiber diameter distribution using Image J software. Additionally, the fibers were characterized using a fluorescence microscope to verify the functional integration of GFP-HABP fusion proteins into the nanofibers via the GFP fluorescence existence. Control and protein-infused fibers were imaged using a 4× objective on a multimodal plate reader (Cytation3, BioTek, Winooski, VT, USA) and fluorescence intensity within the fibers was quantified using associated Gen5 software.

2.5.2. Fourier Transform Infrared Spectroscopy

The infrared spectra of fibers were recorded on a Perkin Elmer Spectrum-400 FTIR spectrometer at the ambient temperature between 4000–650 cm^{-1} with a resolution of 4 cm^{-1}. To obtain reasonable signal to noise ratio the average of 20 scans was taken. Samples were analyzed directly on a single bounce diamond (ATR).

2.5.3. Dynamic Mechanical Analysis (DMA)

Samples subjected to DMA were cut from the aligned fiber films into rectangular specimens of approximately 30 mm × 6.5 mm × 0.25 mm. Analyses were carried out using a DMA (Q800 from TA Instruments) in the film tension mode with an amplitude of 10 µm, a frequency of 1 Hz, a force track of 125%, and a heating rate of 2 °C min^{-1}. The α-relaxation temperature, T_α is defined at the loss modulus peak.

2.5.4. Measurements of Shape Memory Properties

The samples (fiber mats) were heated with a hot plate, and then the samples were bended to a certain angle once the temperature reached the stretching temperature (flat to bent). Thereafter, the samples were cooled down very quickly (with a high cooling rate of 10–20 °C min^{-1}) to a temperature lower than 30 °C. Finally, they were heated again. The deformed sample subjected to a lower heating rate, and the shape recovery can be observed as the temperature reached a certain point. The whole process of shape memory testing was recorded using a digital video and the frames of the video was used to calculate the deformed angle at various time intervals, which can be used to evaluate the value of recovery ratio. The stretching temperatures used were 74, 82, 92, or 104 °C. Generally, 74 °C was mostly used because it is quicker to cool down from this point compared with others. The heating rate was varied between 10 and 20 °C min^{-1}. For quick cooling down, after deformation at the stretching temperature, an ice bath was used rather than just blowing air on it. The heating rate of second ramp was set lower than for the first time, it was set around 5–10 °C min^{-1}.

2.5.5. Raman Spectroscopy

Following biomineralization experiments, fibers were removed from the biomineralization buffer and allowed to dry, under ambient conditions. Several segments of mineralized and control fibers with and without the GFP-HABP protein were analyzed using confocal micro-Raman spectroscopy (Horiba JobinYvon-LabRam ARAMIS Micro-Raman) to determine changes in the chemical composition of the fibers. Reference spectra were first collected for untreated fiber samples to identify a characteristic composition of the PLLA/PMMA fiber scaffold. Raman features associated with the polymeric scaffold display distinct peaks defined near 812, 875, 970, 983, 1122, and 1454 cm^{-1}. Spectral scans were taken for control and mineralized samples at 3 µm intervals throughout an area of 12 × 15 µm and the point spectra at each location were studied. Raman spectral features associated with hydroxyapatite mineral (590, 960, 1044, and 1074 cm^{-1}) were compared across all regions to assess compositional differences across all samples. Peak ratios were taken of the 960 and 812 cm^{-1} bands to draw comparisons regarding the biomineralization differences between all samples.

3. Results and Discussion

3.1. The Morphologies of PLLA/PMMA Fibers/Mats

The morphology of fibers revealed bead-free, continuous, uniform structures (Figure 2a,b). Single strand pore-free
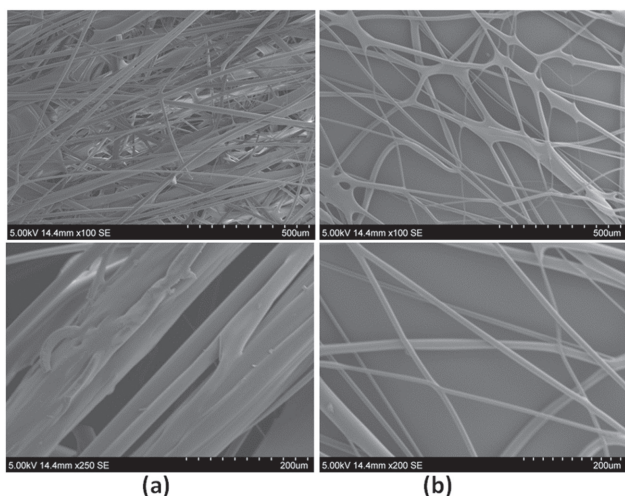
Figure 2. Scanning electron micrographs of 50 wt% PLLA/50 wt% PMMA fibers prepared at a rotating speed of 36 000 rpm under different pressure a) 0.1 MPa, b) 0.2 MPa.

fibers were bundled together and it was also possible to form well-aligned structures due to the high stretching force experienced during gyration. The interconnection of fibers led to formation of a network-like structure. This may be due to a "fingering instability" at the orifice of the gyration vessel that may not have sufficient shear force to generate break-off of individual fibers.[11] Generally, solvents with a high boiling point evaporate slowly and this causes stretching of a polymeric jet.[21] The fusion of polymer fibers at junctions may be due to solvent evaporation and the variation in solvent evaporation rate in blended fibers. The lower boiling point solvent, (chloroform, 61 °C in this case) has little time to evaporate and solidifies quickly during the spinning process resulting in fusion of fibers at the junction. It is also noteworthy that defect-free fiber morphologies could be

produced when the concentration is 2–2.5 times the C_e (the implications of the entanglement concentration).[22] It is very interesting to note that surface of the fibers are pore-free and uniform across all mats. Generally, blended polymeric structures generate porous structures by having different phases that separate from each other due to immiscibility. However, the results here show that the PMMA/PLLA phases are having good miscibility in the chloroform preventing porous structure formation. Additionally, the functionality of the incorporated chimeric protein was determined via measuring the changes in the fluorescence intensity in the region for GFP that is used as a monitoring tool to verify the localization of the hydroxyapatite binding peptide, i.e., HABP. Because the blended polymer scaffolds also display auto-fluorescence in the green region, the intensity was normalized for GFP-HABP-containing fibers with respect to control samples. Figure 3 shows fluorescent images of chimeric protein containing fibers. Engineered protein infused fiber scaffold resulted in 20% increase in the average fluorescence intensity when compared to the polymer only control samples. This enhanced and homogenously distributed fluorescence intensity demonstrates the incorporated protein still remains active following introduction to solvents and the polymerization process, resulting in a bioactive fiber.

The fiber diameter analysis of the spun products show an average fiber diameter of 17 µm at a rotating speed of 36 000 rpm and 0.1 MPa working pressure (Figure 4).

3.2. Thermal-Mechanical Analysis of the PLLA/PMMA Fibers

Figure 5a shows the storage and loss modulus of the blended fibers as a function of temperature. The storage modulus of the blended fibers initially increased with increasing temperature and reached a maximum value at 45 °C, thereafter it decreased with increasing temperature.
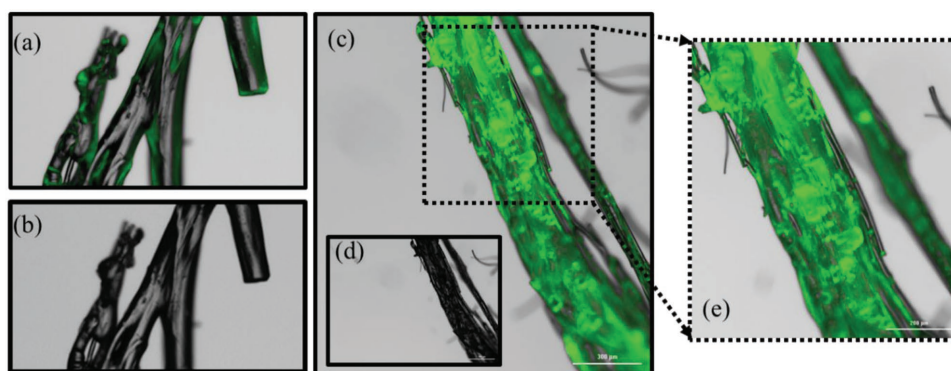

Figure 3. a) Fluorescence and b) bright field microscopy images of PLLA/PMMA fibers only. c) Fluorescence and d) bright field microscopy images of PLLA/PMMA fibers functionalized with GFP-HABP and e) zoom out image showing the fluorescence intensity is homogenous throughout the protein functionalized fiber.
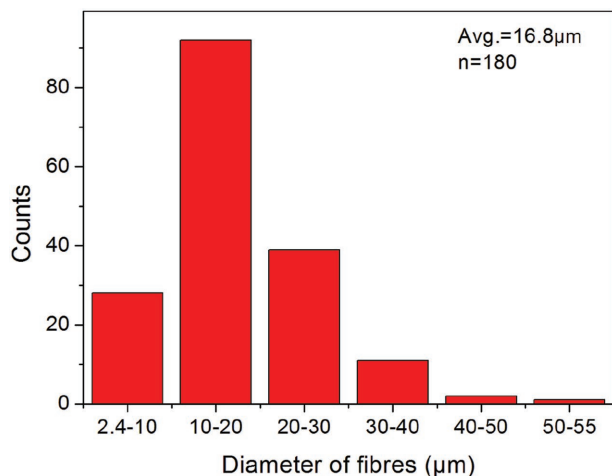
**ADVANCED
SCIENCE NEWS**

www.advancedsciencenews.com

Figure 4. Fiber diameter distribution of 50 wt% PLLA/50 wt% PMMA fibers made at a rotating speed of 36 000 rpm and pressure of 0.1 MPa.

The loss modulus and the loss factor may be used interchangeably to measure the characteristic temperatures pertaining to various relaxation processes. Figure 5a shows two different peaks recorded at 60 and 80 °C. This demonstrates that two different continuous phases appear in the blended fibers at a microscopic level. Actually, these two peaks are related to the glass transition temperature of the PMMA rich phase and the PLLA rich phase in the blended fibers. Generally, microstructure of these blended fibers depends on the weight ratio of original polymers. A transition from polymer rich phase to bicontinuous core/shell structure occurs when the weight ratio increases from 100:0 to 40:60. However, further increase of the weight ratio will result in discontinuous phase.[23,24] Moreover, phase separation of polymers depends on the environmental conditions during spinning. At higher relative humidity, the rate of solidification is faster due to water molecules which will act as a non-solvent to polymers. Thus, this leads to higher phase separation than the conditions found at lower relative humidity.[25] Figure 5b shows the stress–strain behavior of the blended polymer fibers as a function of temperature. The stress (or strain) of the fiber mats were increasing with temperature and shows a maximum value at 45 °C. The stress measured at this temperature was 1.25 MPa with a corresponding strain of 0.25%. Further increasing the temperature reduced the stress (or strain) of the blended polymeric fibers. In Figure 5b, the corresponding tan δ (damping factor) shows a peak between 80 and 90 °C and this is due to glass transition of blended fibers.

3.3. Shape Memory Properties of the PLLA/PMMA Mat

Figure 6 demonstrates the shape memory effect of the blended polymeric mat. At time 0 s, a flat fiber mat was bent and was observed at a temperature of 74 °C. A gradual recovery process (to flat) occurred and was recorded at different time intervals (every 15 s) up to 150 s. It indicates that the mat clearly recovers its original position and a video illustrating the events of Figure 6 is given in Supporting Information.

The acute angle of deformation, i.e., the angle between bending surface and the plate plane (shown in Figure 6), and the corresponding strain during each time interval was calculated using digital micrographs and are shown in Figure 7. In the initial heating process, this flat fiber mat is not deformed and the angle is not increased until the temperature reached the stretching point. The angle of deformation increased from 0° to 70° after the temperature reached 82 °C (Figure 7a). Thereafter, it remained constant. In the cooling down process this angle remained almost constant at ≈70° when reducing the temperature from 82 to 33 °C at a high cooling rate (≈10° min⁻¹) (Figure 7b). In the reheating process the angle of deformation was again reduced from 70° to 5° when increasing the temperature from 25 to 88 °C (Figure 7c).

Generally, shape memory polymers show dual-shape memory effect, i.e., they will able to store different shapes including temporary and permanent. For an effective shape memory effect one needs to have chemical and/or physical cross-links in the polymer network. The shape memory effect could be enhanced by inducing
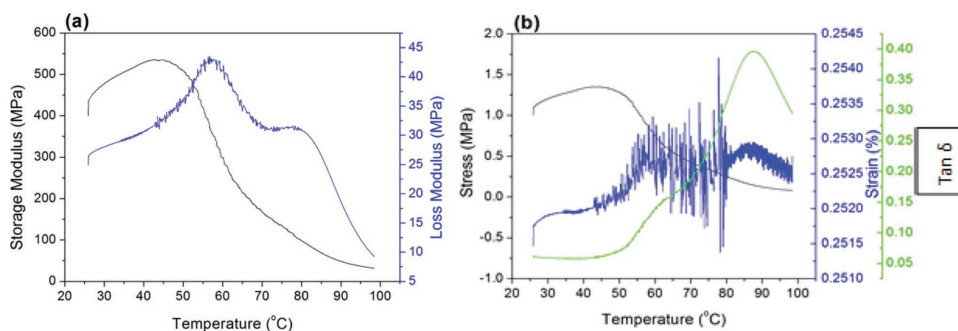

Figure 5. a) Storage and loss modulus of shape memory mats. b) Stress–strain characteristics of PMMA/PLLA fibers and damping factor Tan δ.

**ADVANCED
SCIENCE NEWS**
www.advancedsciencenews.com

Macromol. Biosci. **2017**, *17*, 1600270
© 2016 The Authors. Published by WILEY-VCH Verlag GmbH & Co. KGaA, Weinheim
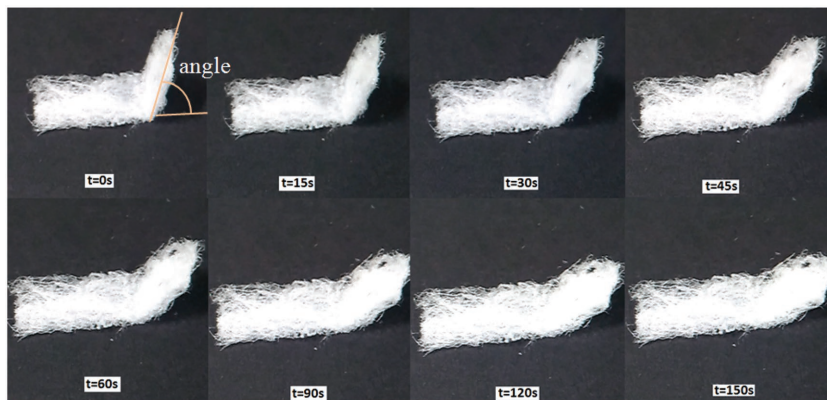
(5 of 8) **1600270**

Figure 6. Demonstration of the shape memory effect of the polymeric mats prepared in this work.

several distinct glassy and/or melting domains within the polymer chains. The dual shape memory effect of the blended fibers is shown in Figure 8. The sample was flat initially, then it was deformed at 94 and 65 °C, respectively, to show the dual shape memory effect. The recovery process of double stretching was observed thereafter where the sample recovers to its original flat position. This indicates that we will able to tune properties of the polymer blend at different temperatures.

3.4. Biomineralization

Both control and protein-containing fiber mat sections were subjected to a 24 h biomineralization assay. Compositional analysis of the mineralized fiber scaffolds was performed via FTIR and Raman spectroscopy. Figure 9 shows the FTIR spectra for the dry fibers before mineralization, fibers incubated in biomineralization buffer only (vehicle control), and fibers which were incubated in biomineralization buffer with the addition of AP enzyme to initiate the mineral formation by releasing phosphate ions into calcium rich environment. The PLLA/PMMA blended fibers have several bands attributed to either PLLA or PMMA individually such as peaks at 988, 865, and 842 cm^{-1}, corresponding to O—CH$_3$ and C—H rocking modes.[26] Due to the overlapping spectral features, notable hydroxyapatite mineral peaks can be observed via shifts in the spectra near 1042 cm^{-1} (v_3), attributed to PO$_4$.[27,28] When comparing the spectral shifts between the control and the protein-infused samples treated with AP enzyme, the GFP-HABP-containing fiber
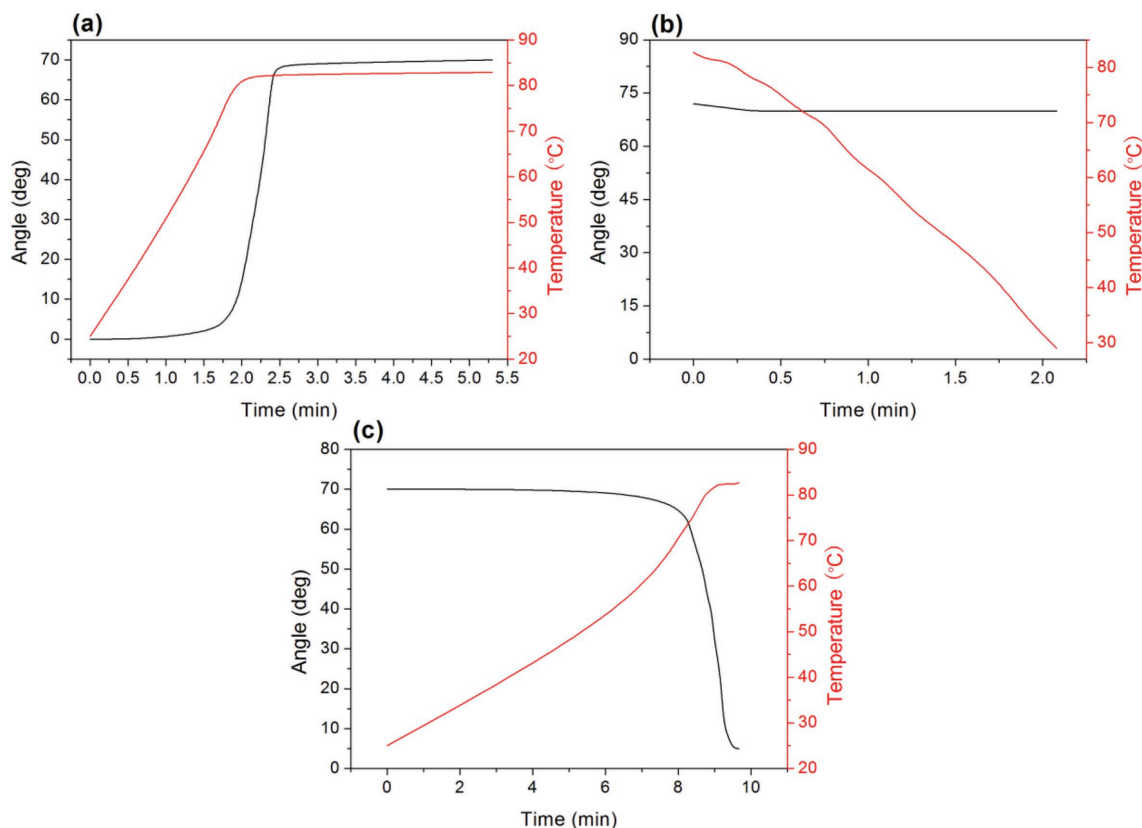

Figure 7. Angle of deformation (representing the corresponding strain) during the heat-cool-heat cycle of the polymeric mats a) heating stage, b) cooling stage, and c) reheating stage.
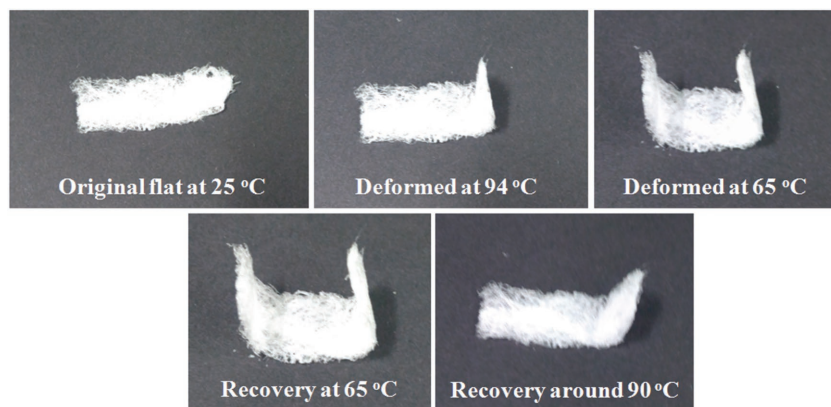
www.advancedsciencenews.com

Figure 8. Demonstration of the double shape memory effect of the polymeric mats prepared in this work.

scaffold displays a very distinct peak at 1040.5 cm^{-1}, which is much nearer to the mineral peak than the control fiber at 1035.8 cm^{-1}. FTIR bands near the defined phosphate peak at 1042 cm^{-1} indicate the mineral formed in the GFP-HABP sample better represent the composition and structure of the natural hydroxyapatite mineral phase.[26–28]

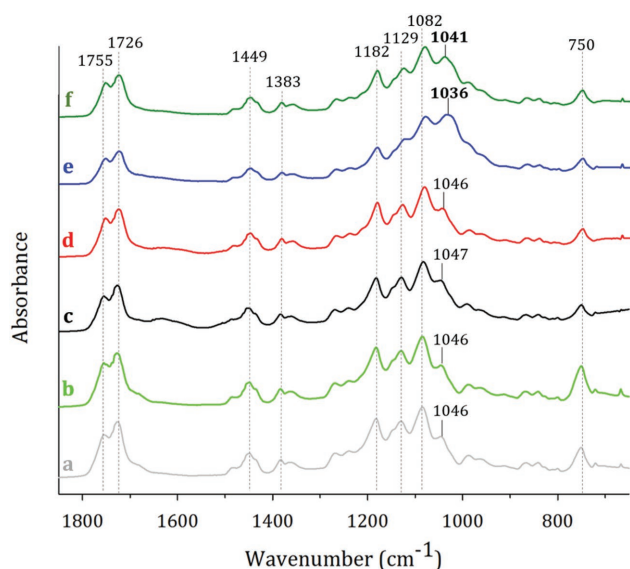Figure 10 illustrates the Raman spectra for both PLLA/PMMA-only and PLLA/PMMA with GFP-HABP fibers

incubated either in biomineralization buffer only (vehicle control) or biomineralization buffer with the addition of AP enzyme to catalyze mineral formation. The peaks at 812 cm^{-1} are associated with C–O–C symmetric stretching of the PLLA/PMMA polymer blend.[29] The bands at 960 cm^{-1} are characteristic of P–O symmetric stretching in phosphate groups, as noted in hydroxyapatite mineral.[28] For each mineralized fiber sample, a ratio was taken of the 960 and 812 cm^{-1} bands to measure differences in the degree of mineralization. For the fibers not treated with the AP enzyme, the band ratios were not significantly different for the PLLA/PMMA fiber when compared to the fusion-protein-functionalized fibers. The addition of AP into the mineralization buffer resulted in an increase in the 960/812 peak ratio, as would be predicted. However, the GFP-HABP-functionalized fiber treated with AP displayed a significantly greater contribution at the 960 cm^{-1} mineral peak (comparatively). This increase following the 24 h biomineralization assay indicates the enhanced production of hydroxyapatite mineral within the GFP-HABP infused SMP fiber scaffold when compared to PLLA/PMMA fibers without the fusion protein.
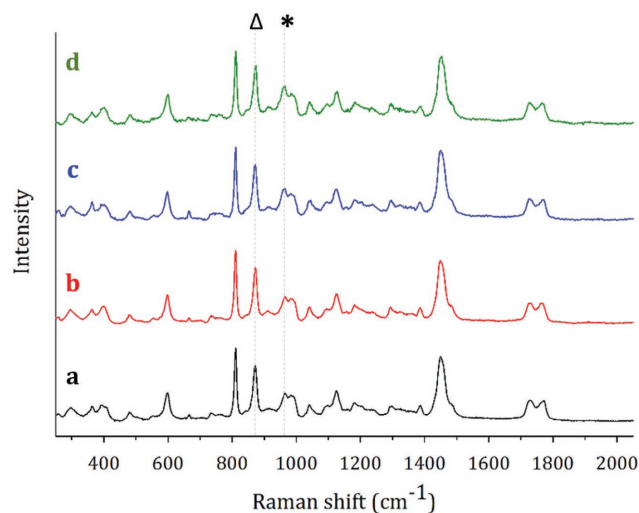

Figure 9. FTIR spectra for PLLA/PMMA only and GFP-HABP-functionalized PLLA/PMMA fibers, respectively, alternating. a,b) Figure includes spectra for the dry fibers before mineralization, c,d) fibers incubated in biomineralization buffer only (vehicle control), and e,f) fibers that were incubated in biomineralization buffer with the addition of enzymatic AP. A significant shift is observed near the peak associated with mineral, 1040 cm^{-1} as shown in the e) PLLA/PMMA only and f) protein-functionalized PLLA/PMMA fibers which were treated with AP enzyme. These samples are shifted from the other spectra which feature bands at about 1046 cm^{-1}.

Figure 10. Raman spectra for biomineralization assay samples. (a,b) represent spectra for vehicle controls samples (no enzymatic AP added) a) PLLA/PMMA only fiber and b) the PLLA/PMMA fiber with GFP-HABP. Raman spectra for the mineralized fibers are shown as (c) and (d) for c) PLLA/PMMA only fiber and d) GFP-HABP-functionalized PLLA/PMMA fiber. Line at Δ represents a band associated with PLLA at 875 cm^{-1}. Reference line at* indicates spectral features occurring at the 960 cm^{-1} peak, a distinct hydroxyapatite mineral peak.

ADVANCED
SCIENCE NEWS
www.advancedsciencenews.com

Macromol. Biosci. **2017**, 17, 1600270
© 2016 The Authors. Published by WILEY-VCH Verlag GmbH & Co. KGaA, Weinheim

(7 of 8) **1600270**

4. Conclusions

PLLA/PMMA composite shape memory fibers were successfully spun using pressurized gyration. The shape memory effect of the fibers was evaluated using a heat-cool-heat cycle. Incorporation of the green fluorescence protein engineered with hydroxyapatite binding peptide into the binary blend fibers resulted in bioactive shape memory fibers using this process. The bonding characteristics of the fiber-proteins were determined. Enzyme based biomineralization studies conducted on the fibers demonstrated that shape memory fibers and mats can have controllable inherent mineralization abilities through integrated bioactivity.

Supporting Information

Supporting Information is available from the Wiley Online Library or from the author.

[1] F. E. Feninat, G. Laroche, M. Fiset, D. Mantovani, *Adv. Eng. Mater.* **2002**, *4*, 91.

[2] A. Lendlein, S. Kelch, *Angew. Chem. Int. Ed.* **2002**, *41*, 2034.

[3] S. Cedric, B. Sophie, L. Jean-Marc, R. Jean-Marie, D. Philippe, *Macromolecules* **2014**, *47*, 6791.

[4] E. M. Woo, Y. H. Wang, *Macromol. Chem. Phys.* **2012**, *213*, 1688.

[5] L. B. Peres, L. B. Peres, P. H. H. Araújo, C. Sayer1, O. H. Gonçalves, *Polímeros* **2015**, *25*, 23.

[6] M. Avella, M. E. Errico, B. Immirzi, M. Malinconico, L. Falcigno, L. Paolillo, *Macromol. Chem. Phys.* **2000**, *201*, 1295.

[7] C. Samuel, J. M. Raquez, P. Dubois, *Polymer* **2013**, *54*, 3931.

[8] J. Eckelt, S. Enders, M. D. Goncalves, D. P. Queiroz, B. A. Wolf, *Fluid Phase Equilib.* **2000**, *171*, 219.

[9] J. Shen, W. Jiang, Y. Liu, R. Wei, X. Liu, Y. Zhong, J. Xu, L. Li, G. Xue, *J. Appl. Polym. Sci.* **2012**, *124*, 3905.

[10] S. Hirota, T. Sato, Y. Tominaga, S. Asai, M. Sumita, *Polymer* **2006**, *47*, 3954.

[11] S. Mahalingam, M. Edirisinghe, *Macromol. Rapid Commun.* **2013**, *34*, 1134.

[12] S. Mahalingam, B. Raimi-Abraham, Q. C. M. Duncan, M. Edirisinghe, *Langmuir* **2014**, *31*, 659.

[13] M. Orlu-Gul, A. A. Topcu, T. Shams, S. Mahalingam, M. Edirisinghe, *Curr. Opin. Pharmacol.* **2014**, *18*, 28.

[14] S. Mahalingam, Z. Xu, M. Edirisinghe, *Langmuir* **2015**, *31*, 9771.

[15] S. Mahalingam, B. T. Raimi-Abraham, D. Q. M. Craig, M. Edirisinghe, *Chem. Eng. J.* **2015**, *280*, 344.

[16] S. Mahalingam, G. G. Ren, M. Edirisinghe, *Carbohydr. Polym.* **2014**, *114*, 279.

[17] S. Mahalingam, G. Pierin, P. Colombo, M. Edirisnghe, *Ceram. Int.* **2015**, *41*, 6067.

[18] Z. Xu, S. Mahalingam, P. Basnett, B. Raimi-Abraham, I. Roy, D. Craig, M. Edirisinghe, *Macromol. Mater. Eng.* **2016**, *301*, 922.

[19] E. Yuca, A. Y. Karatas, U. O. Seker, M. Gungormus, G. Dinler-Doganay, M. Sarikaya, C. Tamerler, *Biotechnol. Bioeng.* **2011**, *108*, 1021.

[20] M. Gungormus, H. Fong, I. W. Kim, J. S. Evans, C. Tamerler, M. Sarikaya, *Biomacromolecules* **2008**, *9*, 966.

[21] C. L. Pai, M. C. Boyce, G. C. Rutledge, *Macromolecules* **2009**, *42*, 2102.

[22] M. G. McKee, G. L. Wilkes, R. H. Colby, T. E. Long, *Macromolecules* **2004**, *37*, 1760.

[23] A. J. P. Bauer, Y. Wu, B. Li, *Macromol. Biosci.* **2016**, *16*, 705.

[24] A. J. P. Bauer, T. Zheng, J. Lu, C. Uthaisar, B. Li, *Macromol. Rapid Commun.* **2014**, *35*, 715.

[25] C-L. Pai, M. C. Boyce, G. C. Rutledge, *Macromolecules* **2009**, *42*, 2102.

[26] C. Samuel, S. Barrau, J. M. Lefebvre, J. M. Raquez, P. Dubois, *Macromolecules* **2014**, *47*, 6791.

[27] C. C. Silva, A. G. Pinheiro, M. A. R Miranda, J. C. Goes, A. S. B Sombra, *Solid State Sci.* **2003**, *5*, 553.

[28] J. Chen, B. Chu, B. S. Hsiao, *J. Biomed. Mater. Res. A* **2006**, *79*, 307.

[29] K. Vano-Herrera, A. Misiun, C. Vogt, *J. Raman Spectrosc.* **2015**, *46*, 273.

ADVANCED
SCIENCE NEWS
www.advancedsciencenews.com